Measurement of a 2-meter flat using a pentaprism scanning system

Proteep C. V. Mallik
Chunyu Zhao
James H. Burge
University of Arizona
College of Optical Sciences
Tucson, Arizona 85721

Abstract. Precise manufacturing of optical flats requires precise characterization of the surface. A scanning pentaprism system is ideal for use as an absolute and precise test for an optical flat. Such a system was built and used to test a 2-m diameter flat mirror. This system uses light from an autocollimator that is reflected from two pentaprisms to project reference beams of light onto the flat mirror. The light reflected from the mirror back through the pentaprisms provides information on low order optical aberrations in the flat mirror. We report results of the test on a 2-m flat, characterizing the errors and their sources. There is enormous potential for our system to be used to test larger flats and even curved surfaces, made of either a glass or a liquid. © *2007 Society of Photo-Optical Instrumentation Engineers.* [DOI: 10.1117/1.2700386]

Subject terms: pentaprism; flat mirror; optical testing; optical scanning; difference measurements; slope measurements.

Paper 060354R received May 10, 2006; revised manuscript received Jul. 26, 2006; accepted for publication Jul. 31, 2006; published online Feb. 20, 2007. This paper is a revision of a paper presented at the SPIE conference on Optical Manufacturing and Testing VI, July 2005, San Diego, California. The paper presented there appears (unrefereed) in SPIE proceedings Vol. 5869.

1 Introduction

The precise optical testing of large flats using a large reference sphere, as in the Ritchey-Common test,[1] is often impractical. Interferometric methods for testing require a good quality reference surface of matched topography. A method using a scanning pentaprism[2] is a convenient way to obtain information on low order aberrations of an optical flat. [*Low order* refers to low spatial frequency errors (<0.1 mm^{-1}), which are sometimes referred to as *form errors, figure errors*, and *topography* in the literature.] The scanning pentaprism test is not new and has been used as an end-to-end test of telescopes.[3–5] It has also been used to make ultraprecise (subnanometer) surface topographic measurements.[6–8]

Unlike interferometric tests, which are instantaneous, scanning tests involve data collected over a considerable amount of time. This is a noncontact test. Furthermore, it is an absolute method that does not rely on a high quality reference surface.

A pentaprism may be used to relay a collimated beam from an autocollimator to the mirror surface. The angle between the reflected beam relayed back to the autocollimator and the beam exiting the autocollimator is a direct measure of the surface slope of the mirror. The pentaprism may be scanned in a line along the surface to get a series of slope measurements. Integrating the measurements gives the surface profile along the scan direction. Several such scans may then be stitched together to get complete information about the mirror surface.

The unique advantage of using a pentaprism is that it deviates light by exactly 90 deg regardless of the orientation of the pentaprism to the incident beam from the autocollimator [Fig. 1(a)]. Thus, the resulting measurements are independent of prism alignment. For this reason, scanning pentaprisms have also been used in optical pick-up heads[9] and in long trace profilers (LTPs)[10] for enhanced system stability.

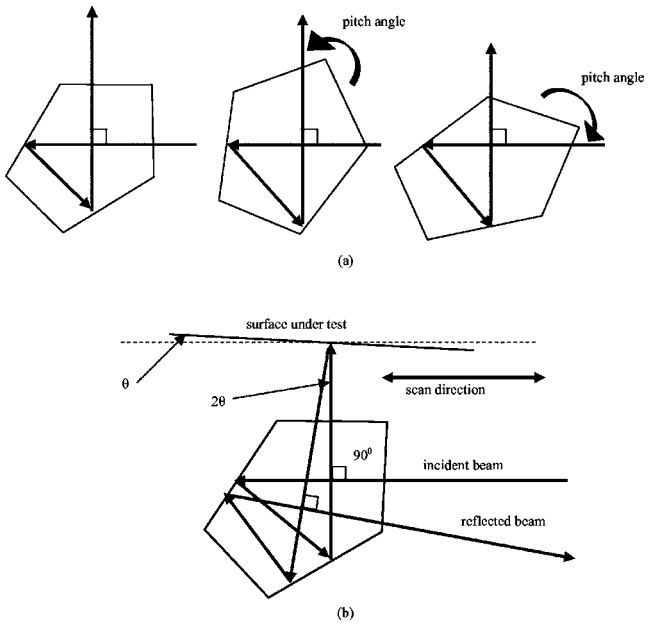

Fig. 1 (a) Principle of a pentaprism. The prism deviates an incoming beam of light by 90 deg, irrespective of the orientation of the prism in pitch. (b) Angular difference, 2θ, between incident and reflected beams is due to a tilt$=\theta$ in the surface being tested.

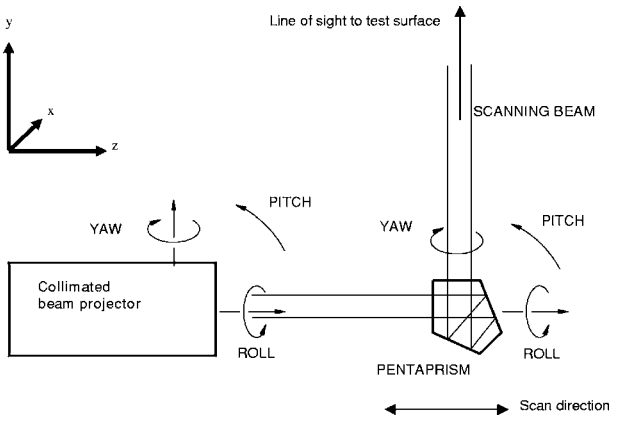

Fig. 2 Degrees of freedom of a pentaprism. Roll is about the *z* axis; yaw is about the *y* axis; and pitch is about the *x* axis.

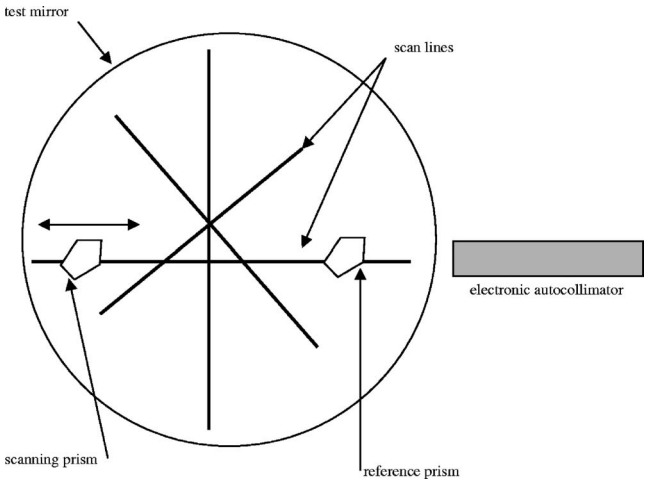

Fig. 4 To obtain information on low order aberrations of the full test surface, multiple linear scans need to be taken.

2 Principles of Operation

Our scanning pentaprism system uses two pentaprisms: a reference or stationary pentaprism ($P1$) and a scanning pentaprism ($P2$). It can be seen that the prisms intercept only a subset of all parallel rays from the test surface. $P2$ can now be scanned across the surface to determine the local slope (tilt) of the surface. Each pentaprism deviates the collimated beam from an electronic autocollimator by 90 deg and relays it to the flat mirror as shown in Fig. 1(b). The 90 deg deviation by a pentaprism is insensitive to its alignment in pitch. Therefore, to the first order, any deviation in the reflected beam from the mirror in the plane of the pitch (also referred to as "in-scan" direction) is caused wholly by tilt variations on the mirror.

Figure 2 defines the degrees of freedom for the prism as roll, pitch, and yaw. Even though the prism suffers finite pitch rotation as it is scanned, the deviated beam has no motion in the pitch direction. This is the essential feature of a pentaprism. $P1$ is kept stationary, relaying the beam to a fixed location on the mirror.

The system operation measures the angular displacement of the spot from the scanning prism relative to spots from the fixed, reference prism. At each position of $P2$, the angular difference between the returns from $P1$ and $P2$ from the mirror is recorded by means of the readout from the electronic autocollimator. Each difference reading between $P1$ and $P2$ is a direct measure of the mirror slope between z_1 and z_2 as shown in Fig. 3. This principle is similar to lateral shearing interferometry as described by Elster[11] and Weingärtner et al.[6] However, instead of using one pentaprism and shearing it, we use two pentaprisms to record the angle difference from two locations on the test surface.

This system of differential measurements is insensitive to vibrations, motion of the autocollimator, and other common path errors.[6] Several scans may be made across the test surface by either rotating the pentaprism system or the test surface itself. This is schematically shown in Fig. 4.

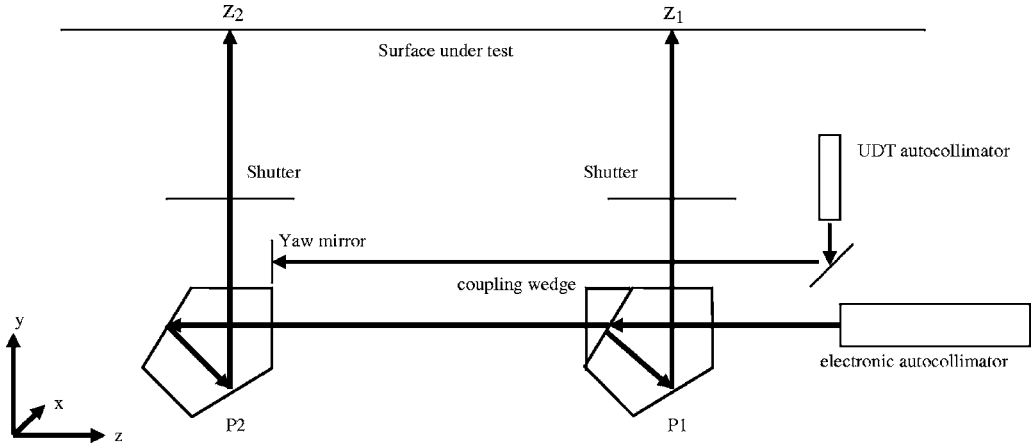

Fig. 3 Schematic of the pentaprism system in an upward staring configuration. Shown are two pentaprisms measuring the tilt of the test surface between two particular locations. Difference measurements, $\theta(z_2)-\theta(z_1)$, are a direct measure of the surface slope between z_1 and z_2. The pentaprism assembly provides accurate measurements only along the scan direction. The UDT autocollimator helps decouple the motion of the scanning prism ($P2$) into yaw and roll components.

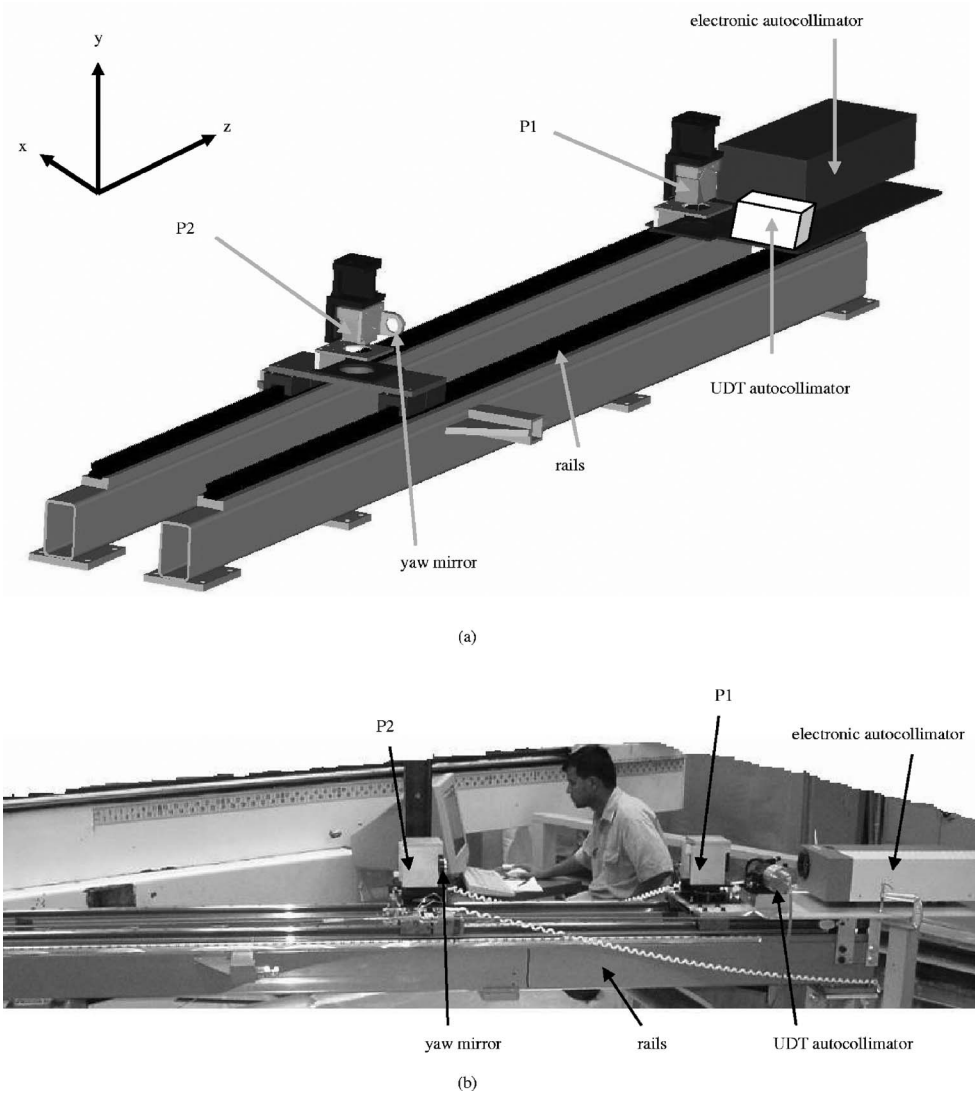

Fig. 5 (a) Shown is a system in downward pointing orientation. The prisms are mounted on movable carriages on a pair of precision-machined rails. (b) The built system is capable of testing 2-m class flats.

3 The System

The scanning pentaprism system was built as shown in Figs. 5(a) and 5(b). The system may be used in either downward pointing (test flat below system) or upward pointing (test flat above system) orientations.

Each pentaprism is in a kinematic mount with picomotor controls for roll and yaw motions. The pentaprisms are fixed onto movable carriages that slide on a pair of precision machined rails along the line of sight of a two-axis electronic autocollimator built by Möller-Wedel (Elcomat 2000). The Elcomat 2000 has an accuracy of 0.5 μrad, with a full measurement range of 10 mrad. It should be noted that the Elcomat corrects for the 2θ tilt internally [see Fig. 1(b)], thereby measuring the surface tilt as is.

There is a mechanical shutter mounted between each prism and the test surface and these are connected through an electronically controlled circuit. The shutters open one at a time, allowing light from only one prism to be incident on the test surface at any given moment.

A collimated beam from an auxiliary two-axis electronic autocollimator (built by UDT Instruments) is aligned to a mirror attached to the mount of $P2$. The purpose of the UDT autocollimator is to decouple the roll and yaw motions of $P2$, which is described in detail in Sec. 4.

The entire system, comprising four picomotors, two electronic autocollimators, and two shutters, is computer-controlled via a LABVIEW interface (see Fig. 6). The 2-m test flat was at the top of an optical test tower, 20 m above the scanning system.

4 Alignment

The accuracy and sensitivity of the scanning system depend critically on the optical alignment of the system. A detailed description of the optical alignment procedure has been given by Mallik et al.[12] Each prism was initially aligned to the Elcomat in roll and yaw to better than 50 μrad. This was accomplished with the use of a helium-neon laser. The prisms were aligned in yaw by overlapping the back reflec-

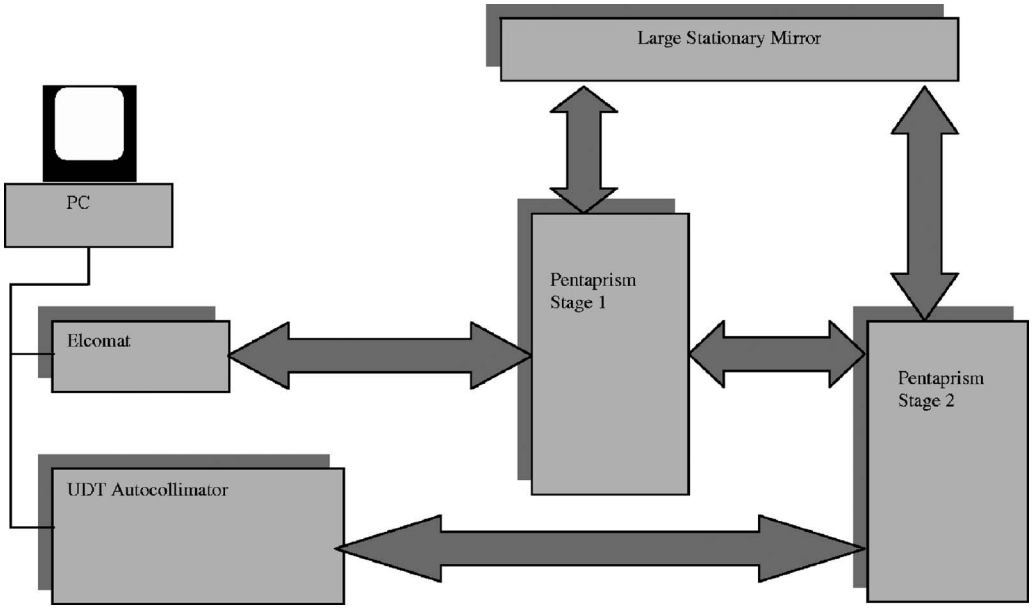

Fig. 6 The pentaprism system is computer-controlled via a LABVIEW interface. The feedback control ensures that the system remains optically aligned during operation.

tions from the surfaces. Roll motion in each prism was used to guide the reflected beam back through the prisms and onto the face of the helium-neon laser. The readout from the Elcomat was used for fine alignment. The influence of yaw and roll motions (x-axis readout) on the in-scan (y-axis) readout was observed. This is a second order effect. The prisms were considered to be aligned to the Elcomat axes when the in-scan readout was insensitive to roll and yaw motions over a range of about 100 μrad.

The mirror attached to the mount of $P2$ helps decouple the motion of $P2$ into yaw and roll components. The optical axis of this mirror is along the z axis (see Fig. 3), so the UDT is insensitive to any movements of $P2$ in roll. However, it is fully sensitive to the motion of $P2$ in yaw. So the yaw component of any misalignment in $P2$ is recovered through the UDT readout, while the Elcomat readout is used to correct for the roll misalignment. A different method is used by Schulz and Weingärtner[13] for accomplishing the same decoupling of motions.

The system is computer-controlled actively via feedback. During the operation of the system, the relative in-scan alignment (pitch errors) between $P1$ and $P2$ is better than 15-nrad rms. The cross-scan alignment (roll and yaw errors) during operation was maintained to better than 50 μrad. The Elcomat alignment to the rails was maintained to better than 50 μrad, resulting in a line-of-sight error in the in-scan direction of less than 10 nrad.

5 Alignment Errors

The performance of the pentaprism system is affected by several sources of alignment errors.[14] The errors are dominated by first order effects and accounting for these is generally adequate because the computed error terms are minimized iteratively by mechanical alignment using the measurements as feedback (Fig. 6). To first order, optical beam pitch and yaw are given by[15]

$$\text{beam pitch} = \text{collimator pitch},$$

$$\text{beam roll} = -\,\text{collimator yaw} + \text{pentaprism roll} + \text{pentaprism yaw}.$$

The second and higher order errors are negligible because they are proportional to the products of two or more errors that are kept small.

Table 1 lists the sources of all line-of-sight errors, up to the second order. The error in the pitch direction varies linearly with beam projector angle (which is common to both prisms) and to second order in other parameters.

The errors and their effects on our measurement results are described in Sec. 8.

Table 1 Contributions to line-of-sight error from prism or beam projector attitude.

Contributions to Line-of-Sight Pitch (In-Scan Direction)	Contributions to Line-of-Sight Roll (Cross-Scan Direction)
Beam projector pitch	Beam projector yaw
(Prism yaw)^2	Prism yaw
(Prism yaw) $\times$ (beam projector yaw)	Prism roll
(Prism roll) $\times$ (beam projector yaw)	(Prism roll) $\times$ (beam projector pitch)
	(Prism yaw) $\times$ (beam projector pitch)

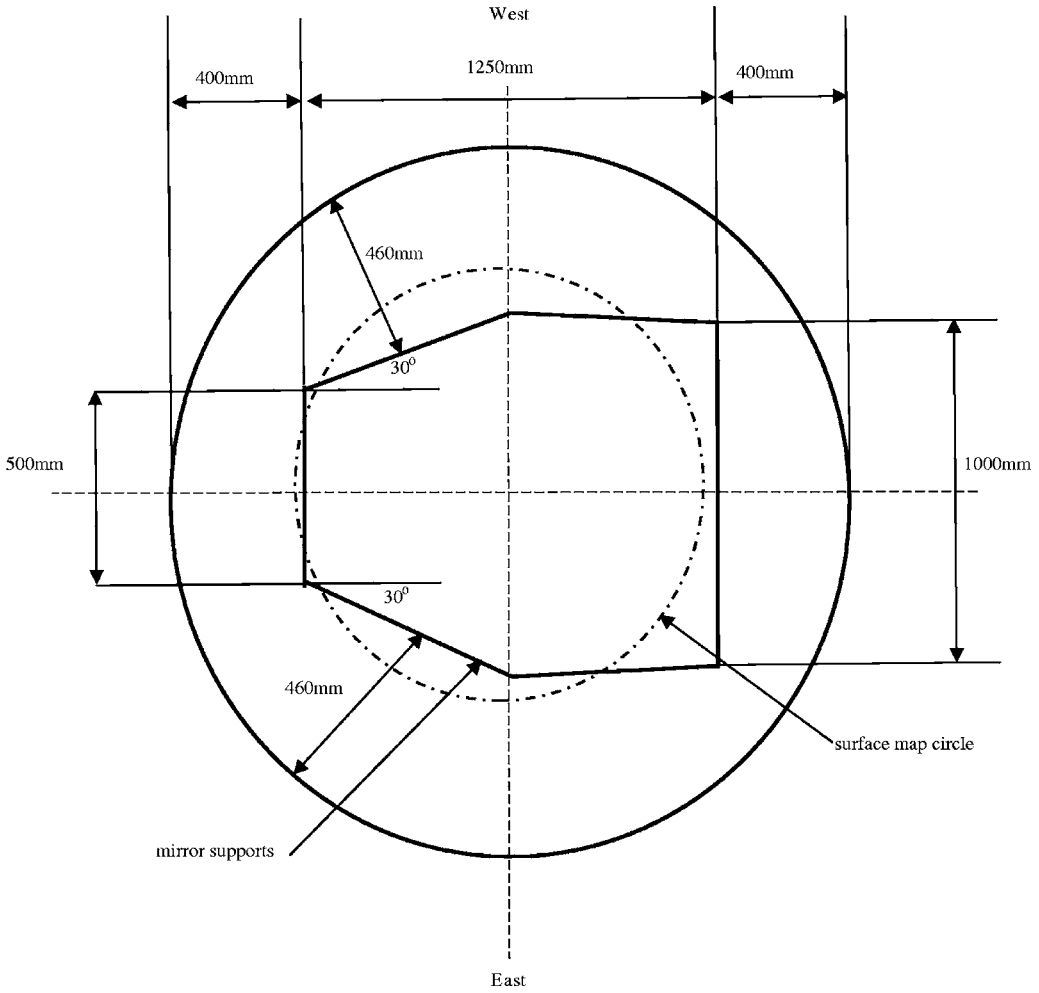

Fig. 7 The dotted circle represents the area being tested. The mirror support structure obscures the rest of the flat. The approximate registration of the six-sided support structure with the test area is also shown. The error in registration of the supports to the test flat is about 25 mm.

6 Measurements

With $P1$ staring at one edge of the test surface, $P2$ was positioned at 50-mm intervals along a scan line. The separation between two scanning points was determined by the Elcomat beam size, which was 50 mm. At each position, slope data on the test surface was collected from the Elcomat. Each data point was calculated as the average of 2500 measurements taken over a time interval of 100 s. Data were collected by letting light through $P1$ for 100 s and then through $P2$ for 100 s. This alternating cycle was repeated several times. There is a short time delay of 10 s between sampling the test and reference prisms. The average time for data collection was determined to be optimal for suppression of noise.

To test for repeatability, data was taken by positioning $P2$ at 50-mm increments along both a forward scan (prism moving in $+z$ direction) and a backward scan (prism moving in $-z$ direction).

After each scan the pentaprism system was rotated by a certain angle about the center of the test flat and a new scan was performed. In this way, a total of six scans were performed. The angles chosen were, clockwise, 0 (oriented north-south), 30, 60, 90, 130, and 150 deg. To obtain data from certain areas not sampled during the initial set of six scans, the 30- and 130-degree scans were extended to the edge of the test flat. This was done by rotating the system by 180 deg from each of those scans and scanning the prism in the opposite direction. These two scans may be considered as additional scans at 210 and at 310 deg.

Figure 7 shows the portion of the mirror surface tested. The mirror supports prevented us from testing the full 2-m aperture, and instead a 1.2-m circle was considered as the well-sampled region being tested.

7 Results

Data from the scans was analyzed using a least-squares fitting algorithm written in MATLAB by Siegel[16] and modified appropriately by the authors. The data was fitted to eight Zernike polynomials, which included power, sine, and cosine astigmatism, sine and cosine coma, sine and cosine trefoil, and spherical aberrations.

The Zernike polynomials are a set of functions that are orthogonal over the unit circle. They are useful for describing the shape of an aberrated wave front in the pupil of an optical system. These polynomials are functions of two

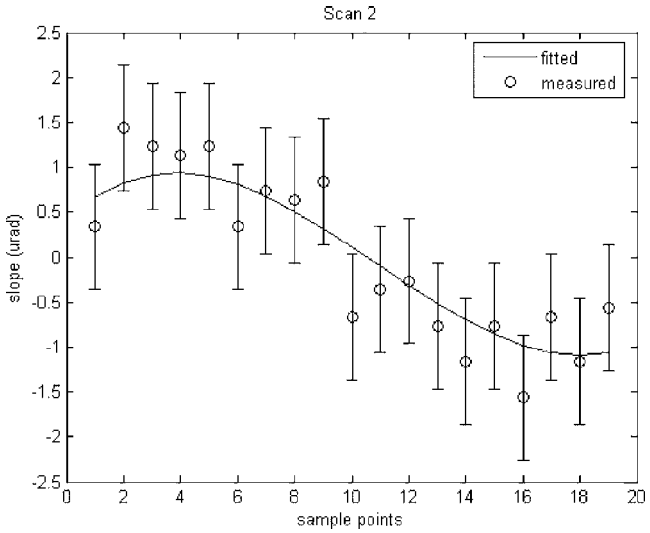

Fig. 8 The fitted curve to the measured data for scan 2 (90 deg scan) is shown here. The error bars correspond to 0.7-μrad rms noise.

variables, $f(\rho,\theta)$, where ρ is the normalized $(0\leqslant\rho\leqslant 1)$ radial distance and θ is the normalized $(0\leqslant\theta\leqslant 2\pi)$ azimuthal angle.

An example of a scan fitted to the eight Zernike polynomials is shown in Fig. 8. The error bars correspond to a rms noise level of 0.7 μrad$=1\sigma$ (the standard deviation). Data from the forward and backward scans vary by considerably less than the noise range. This shows that our system acquires data in a repeatable manner. The sources and analysis of the errors are discussed in Sec. 8. Six such fitted curves are stitched together to form a surface map of the aberrations on the test surface (Fig. 9). From Fig. 9, one can see that our test region was reasonably well-sampled. The trefoil in the surface is consistent with the whiffletree support structure. The results from our test are shown in Table 2 in terms of surface departure from flatness in microns.

A negative sign above corresponds to a convex error. The data may be fitted to higher order Zernike polynomials but with decreasing confidence in the results. The aberrations chosen in Table 2 are the primary aberration terms. These rms wave front aberrations are expressed in terms of Zernike polynomials as follows:[17]

Power: $Z_4=0.577(-1\pm 2\rho^2)$

Cosine astigmatism: $Z_5=0.408\rho^2\cos(2\theta)$

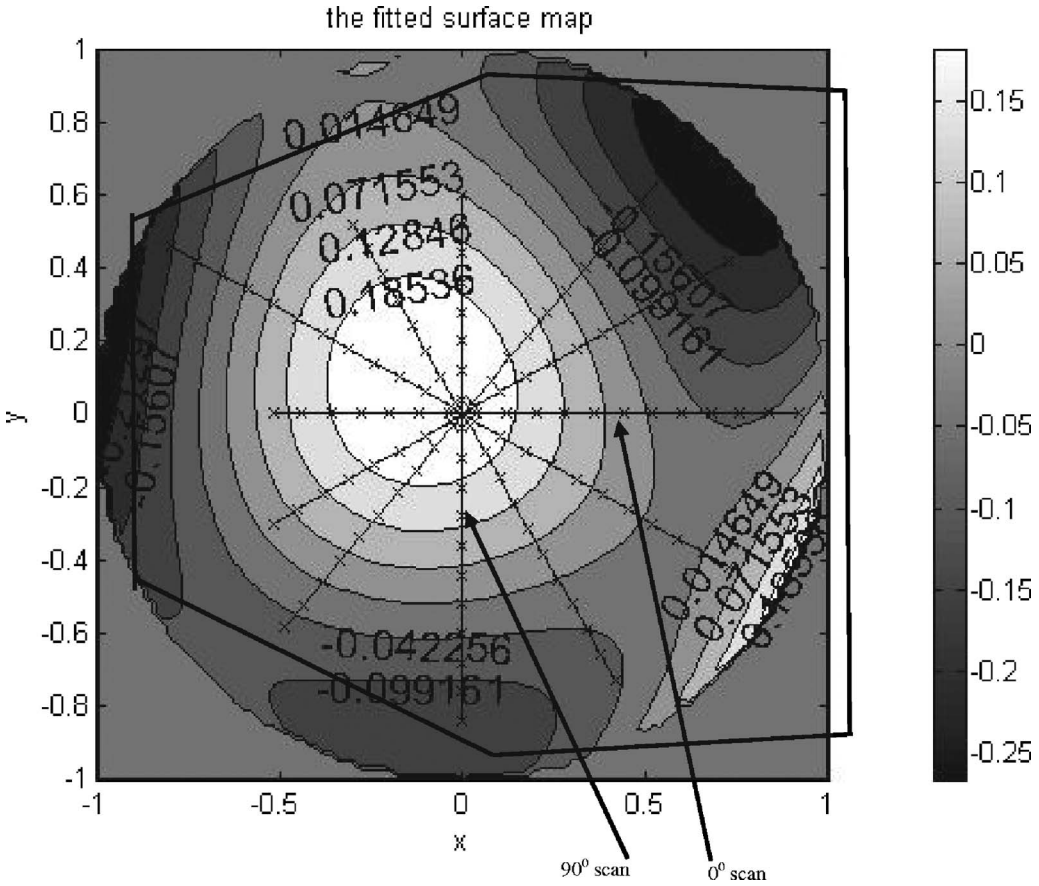

Fig. 9 The surface map above shows the measured pupil aberrations of the test surface over a diameter of 1.2 m. The *x* and *y* axes are normalized to 1, and the color scale is in microns. The six scan lines are also shown, with the *x* marks locating the data points (position of *P*2). An outline of the mirror support structure is superimposed on the surface map.

Table 2 Surface departure: Zernike aberration values are given in microns.

Power	Cos Astig	Sin Astig	Cos Coma	Sin Coma	Spherical	Cos Tref	Sin Tref
−0.091	0.003	−0.033	−0.015	0.025	0.024	0.030	−0.018

Sine astigmatism: $Z_6=0.408\rho^2 \sin(2\theta)$
Cosine coma: $Z_7=0.354\rho(-2+3\rho^2)\cos\theta$
Sine coma: $Z_8=0.354\rho(-2+3\rho^2)\sin\theta$
Spherical (third order): $Z_9=0.447(1-6\rho^2+6\rho^4)$
Cosine trefoil: $Z_{10}=0.354\rho^3\cos(3\theta)$
Sine trefoil: $Z_{11}=0.354\rho^3\sin(3\theta)$

Fitting the data to terms of higher order than the primary aberrations would require better sampling of the test surface.

8 Error Analysis

To characterize the total noise, the pentaprism system was used in a staring mode to look at fixed positions on the test flat over an extended period of time. The rms of the difference between the two prism readings is the noise. Because data for each scan point was taken over a period of less than 10 min, a running average of the noise over this time was found to be 0.7-μrad rms. Our repeatability measurements, described in Sec. 6, agree to within this noise level.

The vibration environment for our system was complex. Short time scale vibrations and drifts were averaged out by our measurements. Long time scale drifts, discussed in Sec. 8.1.1, could not be averaged out sufficiently. Our more recent experiments, in controlled environments, with the pentaprism system have shown that data collected from each prism should be averaged over fewer measurements, and the number of alternating cycles between $P1$ and $P2$ must be increased. The deviation between two successive measurements (separated by 1 s, which is the fastest shutter speed) can be as large as a few microradians, but averaged over 2500 measurements, this deviation should decrease by a factor of 10. However, in reality, we observe a decrease by a factor of 5 or so. This is due to the presence of vibrations and drifts of a whole range of frequencies.

Table 3 Definition of alignment errors for the pentaprism system.

Parameter	Description
Prism yaw	Misalignment of prism in yaw direction due to initial alignment
Δ(Prism yaw)	Variation of yaw orientation for prism
Beam projector yaw	Yaw misalignment of collimated beam relative to direction of motion
Δ(beam projector yaw)	Variation in beam projector line of sight in yaw direction
Prism roll	Misalignment of prism in roll direction due to initial alignment

To better understand the noise in our system, the various error sources and, if available, an estimate of their magnitudes is listed below.

8.1 *Thermal Errors*

It has been shown[16] that a thermal gradient of 0.01 °C/m in the pentaprisms would cause the line of sight to deviate by 20 μrad. Temperature gradients in our test tower caused mainly by the long optical path contribute significantly to our overall error. Long term drift, on the several minute time scale, was also observed in our data due to the bending of the optical tower depending upon the position of the sun in the sky. In controlled lab environments, the pentaprism system routinely acquired data with an intrinsic noise of better than 0.2-μrad rms. Therefore, we can conclude that temperature gradients and other thermal effects contribute almost 0.67-μrad rms of our total noise.

8.2 *Mapping Errors*

A mapping error between the pentaprism position and the location of the beam on the test surface is expected. Given that our test surface is a flat and the local slope variations are not more than 2 nrad/mm, this effect will result in a very small error. If our mapping error is 15 mm, the net error in slope will be 30-nrad rms. Our inability to measure higher frequency errors (though they are small) will contribute to our noise. These unknown errors cannot be removed from our data, and we expect them to introduce up to 30-nrad rms error.

8.3 *Errors from Angular Motion of Prisms and Collimated Beam*

The effects of angular motion and misalignment for the pentaprism system couple to the slope measurements only as second order effects, listed in Table 1. For example, a yaw misalignment by itself will have no effect, but yaw motion in the presence of yaw misalignment will cause a small slope error given by the product of the misalignment and the motion.

The coupling of misalignment and instability into in-scan slope errors is found by differentiating the expressions in Table 1. Table 3 gives a summary of the error terms that couple to the measurements and Table 4 gives the terms that contribute to line-of-sight error in the in-scan direction.

The effect of the above terms on the line-of-sight error is expected to be about 100 nrad rms.

8.4 *Errors from Coupling Lateral Motion of Prisms, Beam Nonuniformity, and Diffraction Effects*

Phase and amplitude variations in the collimated beam do not affect the system performance to first order because these effects are common to both prisms. However, to second order, these variations couple into measurement errors.

Table 4 Change in beam direction with misalignments and perturbations.

2^{*}(Prism yaw) $\times$ Δ(Prism yaw)
(Prism yaw) $\times$ Δ(beam projector yaw)
Δ(Prism yaw) $\times$ (beam projector yaw)
(Prism roll) $\times$ Δ(beam projector yaw)
Δ(Prism roll) $\times$ (beam projector yaw)

Three basic couplings with lateral motion of the prism have been identified and analyzed:

1. coupling of phase errors in the collimated beam with transverse motion of the prism;
2. coupling of diffraction effects in the collimated beam with transverse motion of the prism;
3. coupling of amplitude variations in the collimated beam with transverse motion of the prism.

Transverse motion (perpendicular to scan direction) of the prisms may occur due to bent rails.

Phase errors in the wave front are coupled to prism motion according to the phase slope at the edge of the beam given by,

$$\Delta\alpha = \frac{2\Delta x}{D}\frac{\partial W}{\partial r}$$

where $\Delta\alpha$ is the effective change in beam angle; Δx is pupil shear; D is the pupil diameter; $\partial W/\partial r$ is the wave front slope at the edge.

This effect can be corrected by adjusting the autocollimator so that there is no measurable line-of-sight error as the prism is translated. However, we expect about 50-nrad rms tilt error for a 1-mm peak to valley motion of the prism.

Diffraction effects in the propagating collimated beam also cause some errors. Laboratory experiments have shown that this error can be controlled to about 75-nrad rms tilt. Similarly, intensity variations couple with prism errors to the order of 60-nrad rms tilt. These effects combined introduce an error of about 100-nrad tilt per millimeter of prism lateral shift.

Table 5 Combined effect of all errors.

Error Source	Error (nrad rms)	Explanation
Elcomat measurement uncertainty	75	Instrument specification
Mapping errors	45	Sec. 8.1.2
Thermal effects	670	Sec. 8.1.1
Prism and beam angle variation	100	Table 4
Coupling of lateral motion	100	Sec. 8.1.4
Total (RSS)	690	

Table 6 Noise in surface departure. Zernike aberration values are reported with the corresponding error due to noise.

Aberration	Value ± Error (in microns)
Power	−0.091 ± 0.009
Cos astig	0.003 ± 0.019
Sin astig	−0.033 ± 0.015
Cos coma	−0.015 ± 0.006
Sin coma	0.025 ± 0.006
Spherical	0.024 ± 0.004
Cos tref	0.030 ± 0.019
Sin tref	−0.018 ± 0.017

8.5 *Combined Errors*

Combining the effects of all random errors, we come up with the following error budget estimate shown in Table 5.

8.6 *Effects of Random Errors for Scanning Pentaprism Test*

The random errors affect each slope measurement. A Monte Carlo simulation of the random errors and their effect on the Zernike modes was evaluated. Using MATLAB to generate random noise of about 0.7 μrad for each data point along each scan line, 390 independent noise files were simulated. The pentaprism fitting software was used to analyze each noise file. The result is a measure of our uncertainty for each aberration. For the 390 cases, the uncertainties in each of the Zernike aberration coefficients were found to be normally distributed, as one would expect. The 1σ (standard deviation) uncertainties are reported along with the aberration values in Table 6. These uncertainties correspond to a confidence level of 67% for our test results.

Figure 10 shows a sample histogram of the noise data corresponding to the power term (Z_4). The 1σ deviation is 0.009 μrad. The histogram has a Gaussian-like distribution as expected from the random generation of noise data values.

9 Conclusions and Future Work

The pentaprism test is a reliable absolute test for optical flats. It is, however, a time consuming test. Measurements an order of magnitude better can be made with the use of higher quality pentaprisms in more controlled environments.

We currently use our pentaprism system to measure surface quality of flats during their fabrication and polishing. The data is then used to optimize the surface figuring and polishing procedures. Due to a much smaller optical path length, our overall errors are currently significantly less

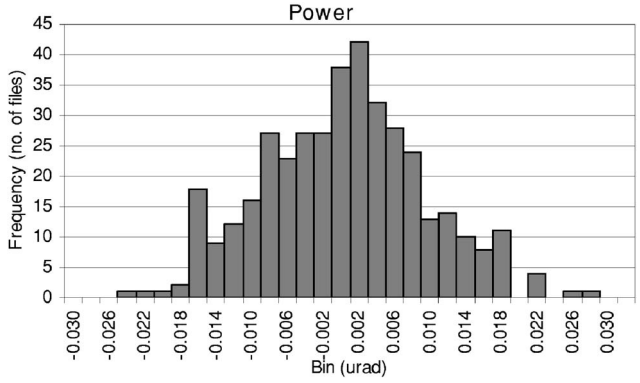

Fig. 10 The histogram for power from 390 randomly generated noise files with rms value = 0.7 μrad. The 1σ deviation is 0.0091 μm.

than those reported in this paper. These measurements show our accuracy to be better than 10-nm rms for low order surface aberrations on a 2-m class flat. Our errors due to noise are also less than 0.1 μrad.

We are also working on using liquid flats to calibrate our pentaprism system. Using two small mercury mirrors separated by a long baseline, we will be able to align our system to a truly flat surface. The gravity-aligned equipotential surface of mercury takes the shape of the local curvature of the earth and our system is able to measure this effect over baselines greater than 1-m. This will enable us to test arbitrarily large flats, glass and liquid, using a calibrated system with significantly reduced errors.

Acknowledgments

The authors would like to thank Andrew Cheng, Jeremy Lusk, Robin Seibel, and Tom Zobrist for their hand in helping run these experiments.

References

1. G. Ritchey, *Smithsonian Contributions to Knowledge*, p. 1459 (1904).
2. N. Hochgraf, "Autocollimator, scanning pentaprism used to measure angular collimation," *Opt. Sci. Cent. Newsl. (Univ. Ariz.)* Jan–Mar, pp. 41–42 (1969).
3. T. Korhonen, "Optics for the Nordic optical telescope," in *Observational Astrophysics, Proc. of Nordisk Forskerkursus*, Copenhagen University Observatory, pp. 198–209 (1987).
4. J. Espiard and B. Favre, "Contrôle en laboratoire de la qualité du systéme optique d'un telescope de 1,524 m de diameter," *Nouv. Rev. Opt. Appl.* **1**(6), 395–400 (1970).
5. R. Wilson, "Matching error (spherical aberration) in the Hubble space telescope (HST): Some technical comments," *ESO Messenger* **61**, 22–24 (1990).
6. I. Weignärtner, M. Schulz, and C. Elster, "Novel scanning technique for ultra-precise measurement of topography," in *Optical Manufacturing and Testing III*, *Proc. SPIE* **3782**, 306–317 (1999).
7. R. Geckeler and I. Weingärtner, "Sub-nm topography measurement by deflectometry: Flatness standard and wafer nanotopography," in *Advanced Characterization Techniques*, *Proc. SPIE* **4779**, 1-12 (2002).
8. M. Wurm and R. Geckeler, "A new method and novel facility for ultra-precise 2D topography measurement of large optical surfaces," in *Optical Metrology in Production Engineering*, *Proc. SPIE* **5457**, 401–410 (2004).
9. W. Sun et al., "Design of miniature HD-DVD optical pick-up head using a penta prism," *J. Mod. Opt.* **52**(5), 775–789 (2005).
10. S. Qian et al., "The penta prism LTP: A long-trace-profiler with stationary optical head and moving penta prism," *Rev. Sci. Instrum.* **66**(3), 2562–2569 (1995).
11. C. Elster, "Recovering wavefronts from difference measurements in lateral shearing interferometry," *J. Comput. Appl. Math.* **110**, 177–180 (1999).
12. P. Mallik, C. Zhao, and J. Burge, "Measurement of a 2-meter flat using a pentaprism scanning system," in *Optical Manufacturing and Testing VI*, *Proc. SPIE* **5869**, 58691A (2005).
13. M. Schulz and I. Weingärtner, "Avoidance and elimination of errors in optical scanning," in *EUROPTO Conference on Laser Metrology and Inspection*, *Proc. SPIE* **3823**, 133–141 (1999).
14. J. Burge, "Internal Technical Memo: Revision E," Optical Sciences Center, University of Arizona (2003).
15. J. Burge, "Advanced techniques for measuring primary mirrors for astronomical telescopes," PhD Thesis, University of Arizona (1993).
16. N. Siegel, "Algorithms for data registration and subtraction in optical testing," MS Thesis, University of Arizona (2005).
17. J. Wyant, "Zernike Polynomials," University of Arizona, (2003); http://www.optics.arizona.edu/jcwyant/Zernikes/ZernikePolynomialsForTheWeb.pdf

Proteep C. V. Mallik received his BS degree in physics and mathematics from the University of Oregon in 2000. He received his MS degree in optical sciences and engineering from the University of Arizona in 2003, and is currently a PhD student working with Professor Jim Burge. His dissertation work is focused on the precision testing of large aspheres using computer-generated holograms. His research interests include adaptive optics, optical fabrication, and optical testing.

Chunyu Zhao earned his BS degree in physics and mechanical engineering (minor) from Tsinghua University in 1993. In 2002, he earned a PhD in optical sciences and engineering from the University of Arizona where he is currently an assistant research professor. His research interest is focused on optical testing and optical design.

James H. Burge received his BS in engineering physics from Ohio State University in 1987, and his MS and PhD degrees in optical sciences in 1991 and 1993, from the University of Arizona. His current position is associate professor at the University of Arizona with joint appointments in optical sciences and astronomy where his interests are astronomical optics, optical fabrication and testing, optomechanics, and optical system engineering.